Corrected: Publisher Correction

Complex lasers with controllable coherence

Hui Cao[1]*, *Ronen Chriki*[2], *Stefan Bittner*[1], *Asher A. Friesem*[2] *and Nir Davidson*[2]*

Abstract | Lasers have enabled scientific and technological progress, owing to their high brightness and high coherence. However, the high spatial coherence of laser illumination is not always desirable, because it can cause adverse artefacts such as speckle noise. To reduce spatial coherence, new laser cavity geometries and alternative feedback mechanisms have been developed. By tailoring the spatial and spectral properties of cavity resonances, the number of lasing modes, the emission profiles and the coherence properties can be controlled. In this Technical Review, we present an overview of such unconventional, complex lasers, with a focus on their spatial coherence properties. Laser coherence control not only provides an efficient means for eliminating coherent artefacts but also enables new applications in imaging and wavefront shaping.

Lasers are widely used in industry, medicine and other areas of contemporary life because of their high brightness, coherence and efficiency and their good spectral control. A laser with high spatial coherence can generate a directional light beam with small divergence, and the beam can be focused onto a diffraction-limited spot. Unfortunately, high spatial coherence also causes deleterious effects such as coherent artefacts and crosstalk in full-field imaging and displays[1]. Coherent artefacts pose serious problems for not just parallel imaging and display applications but also laser applications in materials processing, photolithography, holography and the optical trapping of cold atoms and colloidal particles.

Although various approaches have been developed over the years to suppress deleterious coherence artefacts, they are mostly applied outside the lasers themselves. Such approaches can be summarized as starting with a laser of high spatial coherence and then reducing the spatial coherence of its emission. A direct, more efficient approach is to use a laser with low spatial coherence. Such a laser can be built using unconventional, complex cavities. The study of complex lasers bridges multiple disciplines, including mesoscopic physics, nonlinear dynamics, quantum optics, wave-dynamical chaos and non-Hermitian physics. Thanks to their diversity and versatility, such lasers constitute a toolbox for various applications, which enables application-driven laser design.

In this Technical Review, we discuss the spatial and temporal coherence properties of lasers, with emphasis on spatial coherence. We consider how high spatial coherence can lead to undesirable artefacts and describe unconventional lasers that have inherently low and/or tunable spatial coherence. We also discuss some of the applications for which such lasers are suited.

Laser coherence properties

Conventional lasers (BOX 1) typically have high coherence, but depending on the application, high spatial and/or temporal coherence may not be a desirable property. Coherence can be described by the first-order coherence function, which is a measure of correlations of the electric field E in space and time[2]. It is defined as

$$g^{(1)}(r_1, r_2, \tau) = \frac{|\langle E^*(r_1, t)E(r_2, t+\tau)\rangle|}{\langle E^*(r_1, t)E(r_1, t)\rangle^{1/2}\langle E^*(r_2, t+\tau)E(r_2, t+\tau)\rangle^{1/2}} \quad (1)$$

where r_1 and r_2 are spatial locations, τ is the time difference, * denotes complex conjugation and $\langle\rangle$ denotes averaging over the time variable t for a duration longer than all intrinsic dynamical timescales. The temporal coherence $g^{(1)}(\tau)$ describes the correlation of fields at the same location ($r_1 = r_2$) but at different times, and the spatial coherence $g^{(1)}(r_1, r_2)$ describes the correlation of fields at the same time ($\tau = 0$) but at different locations. The width of $g^{(1)}(\tau)$ gives the coherence time. It is inversely proportional to the spectral width of the laser emission, which depends on the number of longitudinal lasing modes and their linewidth. The width of $g^{(1)}(r_1, r_2)$ gives the coherence length, which is inversely proportional to the number of transverse lasing modes. Hence, the longitudinal modes are also called temporal modes, and the transverse modes are called spatial modes.

[1]*Department of Applied Physics, Yale University, New Haven, CT, USA.*

[2]*Department of Physics of Complex Systems, Weizmann Institute of Science, Rehovot, Israel.*

**e-mail: hui.cao@yale.edu; nir.davidson@weizmann.ac.il*

https://doi.org/10.1038/s42254-018-0010-6

Key points

- High spatial coherence of laser emission, a common feature of conventional lasers, causes deleterious effects, including speckle noise and crosstalk, in applications such as full-field imaging, display, materials processing, photolithography, holography and optical trapping.
- Fundamental changes in laser design or operation are more effective than schemes to reduce the spatial coherence outside of the laser cavity to achieve low or tunable spatial coherence.
- Random lasers and wave-chaotic microcavity lasers support numerous lasing modes with distinct spatial profiles, producing emission of low spatial coherence suitable for speckle-free, full-field imaging and spatial coherence gating.
- The number of modes and thus spatial coherence of degenerate cavity laser emission can be tuned with little change in power, allowing fast switching between speckle-free imaging and speckle-contrast imaging.
- Wavefront shaping inside a degenerate cavity laser can generate propagation-invariant output beams or spin-dependent twisted light beams. The dynamic wavefront control can focus laser light through a random scattering medium.

If the gain material is uniformly distributed in the cavity, the lower-order transverse modes have lower thresholds than the higher-order transverse modes and lase first at lower pump power. They can saturate the optical gain, especially for a homogeneously broadened gain medium, and thus prevent the higher-order modes from lasing at higher pump powers. This effect, known as mode competition, usually determines the number of transverse modes that lase simultaneously and has a profound impact on the spatial coherence of laser emission.

Because of mode competition, commonly used lasers, such as edge-emitting diode lasers, fibre lasers and solid-state lasers, have only a few transverse lasing modes and thus their spatial coherence is usually high. Therefore, one way to reduce spatial coherence is to increase the number of transverse lasing modes. This can be done by reducing the ratio of cavity length to mirror diameter so that the diffraction loss for higher-order transverse modes is reduced, such as for vertical-cavity surface-emitting lasers (VCSELs). Note that the spatial coherence is independent of the number of longitudinal lasing modes that have identical transverse structure. Other approaches will be discussed in the rest of this Technical Review.

High spatial and temporal coherence is not exclusive to lasers. Spatial or spectral filtering of spontaneous emission from a lamp can greatly increase spatial or temporal coherence, albeit at the price of greatly reduced power. A fundamental difference between a laser and a lamp lies in the quantum statistical properties of their emission[3]: on timescales shorter than the characteristic time given by the inverse of the spectral bandwidth, laser light has Poissonian photon statistics, but thermal light has Bose–Einstein statistics.

Speckle suppression

The most common manifestation of coherent artefacts is speckle noise[4,5], which occurs because light fields at different locations are mutually coherent. When these fields are scattered by a rough surface or in a disordered medium, they are scattered to the same position along different paths. Because they are mutually coherent and have random phase delays, these fields interfere to form a random grainy pattern[5]. For a fully developed speckle pattern, the intensity contrast $C = \sigma/\langle I \rangle$ is equal to 1, where σ is the standard deviation of the intensity and $\langle I \rangle$ is the average intensity[4,5].

Because speckles originate from spatial coherence, the most effective way to suppress them is to use light sources with inherently low spatial coherence, such as lamps or light-emitting diodes (LEDs), which have been used for most full-field imaging and display applications. Unfortunately, compared with lasers, these sources have reduced spectral control, poorer collection efficiency and lower power per mode. The power limitations are particularly problematic in imaging applications that involve absorbing or scattering media, which has prompted the use of raster scanning of focused laser spots as an imaging modality[6]. However, scanning is time consuming and thus not suitable for the imaging of moving objects or transient processes.

An alternative way to suppress speckles is to reduce the spatial coherence of light emitted from a laser, for instance, by using a time-varying scattering system such as a rotating diffuser[7], a colloidal solution[8] or a micro-electromechanical mirror array[9]. In the case of a rotating diffuser, different angular positions of the diffuser produce uncorrelated speckle patterns. Summing the intensities of N uncorrelated speckle patterns averages the speckle noise and reduces the speckle contrast[4,5] by a factor of $\sqrt{N}$ (FIG. 1a). However, lowering the speckle contrast below the level of human perception[10,11] ($C < 3\%$) requires summing approximately 1,000 different speckle patterns. It takes time to create that many speckle patterns, and the imaging speed is limited by the velocity of the mechanical motion of the scattering system.

Broadband sources with low temporal coherence, such as superluminescent diodes and supercontinuum sources, have also been exploited for speckle suppression. These sources have high spatial coherence, and only moderate speckle suppression is achieved[5]. For example, when broadband light illuminates a static diffuser, the speckle patterns for different wavelengths are simply linearly rescaled versions of the same pattern (FIG. 1b). Therefore, summing the intensities of speckle patterns for different wavelengths has a limited effect on speckle suppression. Quantitatively, the spectral correlation function characterizes the degree of correlations among speckle patterns for different wavelengths. The spectral compounding is sufficient for speckle reduction only when the illumination bandwidth $\Delta\omega$ is much larger than the spectral correlation width $\delta\omega$. The speckle contrast $C \approx 1/\sqrt{\Delta\omega/\delta\omega}$ reaches 3% for $\Delta\omega \approx$ 1,000 $\delta\omega$. For a standard diffuser, the spectral correlation width is typically a few nanometres in wavelength[12], and reducing C to 3% requires an extremely broadband source. A possible alternative approach is to drastically reduce $\delta\omega$ using multiple scattering events in a thick diffusive medium or a long multimode fibre. However, it is difficult to adopt this method for applications that rely on narrowband lasers, such as excimer lasers for deep ultraviolet photolithography, or that require compact sources, such as red–green–blue lasers for portable displays.

Box 1 | **Conventional lasers**

Here, we describe some fundamental features of conventional lasers with stable cavities. Traditionally, a stable laser cavity is composed of two spherical mirrors facing each other and a gain medium[95]. Light bouncing back and forth between the mirrors is amplified by stimulated emission of the gain medium during each passage. The gain medium is pumped electrically by a current source or optically by a flash lamp or another laser source. At least one of the spherical mirrors is only partially reflective and so a portion of the light leaves the cavity every round trip, thereby producing an output beam. When the light amplification is strong enough to compensate for the loss due to cavity leakage and material absorption, lasing oscillations occur in the cavity.

The spatial field profile of the light must be identical after propagating one round trip through the cavity. This resonance condition determines the field distributions of cavity modes. The number of field nodes in the longitudinal direction, that is, along the cavity axis, gives the longitudinal quantization number, also called the longitudinal mode number. The numbers of nodes in the two orthogonal transverse directions give the two transverse mode numbers. Modes with low quantization numbers are known as low-order modes; modes with high quantization numbers are known as high-order modes.

The light leakage from the cavity is characterized by the quality (Q) factor, which is proportional to the photon lifetime in the cavity and inversely proportional to the round-trip loss. Diffraction loss occurs if the cavity length, that is, the distance between the two mirrors, is much larger than the cavity width, that is, the transverse size of the mirrors. Higher-order transverse modes have finer spatial features and larger transverse wavevector components and thus suffer stronger diffraction loss and have lower Q factors than the lower-order modes. Hence, it is typically the lower-order modes that lase.

Lasers with tunable spatial coherence

To overcome the natural tendency towards high spatial coherence exhibited by conventional lasers, fundamental changes in the laser design or operation are necessary to achieve low or even tunable spatial coherence. In this section, we discuss three strategies to reduce the spatial coherence of lasers. Because only modes with different spatial emission profiles contribute substantially to the reduction in spatial coherence, the first strategy is to drastically increase the number of transverse lasing modes by modifying the laser cavity design. This is implemented, for example, in degenerate cavity lasers or large-mode-area fibre amplifiers, as discussed below.

The second strategy we discuss, which is more radical than the first, is to have many lasing modes with different spatial emission profiles. Most laser cavities, including degenerate cavity lasers or large-mode-area fibre amplifiers, feature a separable geometry with an optical axis that defines the dominant propagation direction, from which results the distinction between longitudinal and transverse modes. However, in laser cavities without an optical axis or separable geometry, individual lasing modes have no dominant propagation direction and can no longer be assigned longitudinal and transverse quantization numbers. Instead, each mode consists of many plane wave components with different directions, and, as a result, all modes can have distinct emission profiles. This approach avoids having a number of different longitudinal lasing modes that do not contribute to the reduction in spatial coherence. We discuss the implementation of this strategy with cavities in the shape of chaotic billiards or with disordered scattering media.

The main challenges for these two strategies are to ensure that different spatial modes have similar Q factors and that their competition for gain is minimal so that they can lase simultaneously. An important advantage is that both strategies can be adapted to different gain materials.

The third strategy does not rely on exciting many distinct spatial modes but instead aims at disrupting the formation of lasing modes in the first place. To this end, the cavity itself is not modified, but instead, the pumping conditions are adjusted such that the cavity is constantly modified by thermal effects and the lasing modes cannot build up. Consequently, the emission is spatially incoherent. We discuss the example of large-aperture VCSELs.

Degenerate cavity lasers. For a large number of transverse modes to lase simultaneously, they must have similar lasing thresholds. This can be achieved with a degenerate cavity laser (FIG. 2), in which all transverse modes have nearly identical Q factors[13,14]. A degenerate cavity forms a self-imaging system (FIG. 2a). Two lenses in a $2f$–$2f$ telescope arrangement are placed between two flat mirrors so that an arbitrary field distribution at any plane in the cavity is imaged onto itself after one round trip. Therefore, any field distribution is an eigenmode of the cavity, and all (orthogonal) eigenmodes are degenerate. Because the lasing thresholds of the transverse modes are nearly identical, all transverse modes can lase simultaneously. It has been shown that a degenerate solid-state laser can support more than 10^5 transverse modes lasing simultaneously and independently, producing emission with extremely low spatial coherence[15].

The number of transverse lasing modes is given by the ratio of the gain medium cross section to the diffraction-limited area that is determined by the smallest numerical aperture of the optics inside the cavity. To tune the degree of spatial coherence, the number of transverse lasing modes can be varied by inserting a variable circular aperture in the mutual focal plane of the two lenses (FIG. 2b). The aperture acts as a spatial filter that introduces loss to higher-order transverse modes[15]. When the aperture is sufficiently small, only the lowest-order transverse mode lases. Because the spatial overlap of the lasing mode and the gain medium remains the same, the total power extracted from the gain medium is nearly unchanged. By decreasing the size of the aperture, the number of transverse lasing modes can be reduced from 320,000 to 1, whereas the output power decreases by less than 50%.

The remarkable efficiency of redistributing energy over 10^5 transverse modes is unique to the degenerate cavity laser (FIG. 2d) and not possible with conventional laser resonators. In a conventional stable laser resonator, the cavity geometry dictates the characteristic mode size, and spatial filtering, for example, with a circular aperture, introduces loss in all modes because of the mismatch between mode size and filter. Consequently, the total power scales linearly with the number of transverse modes, assuming all modes have equal power. By contrast, the modes in a degenerate cavity can have arbitrary transverse profiles, that is, there is no inherent transverse mode size, and the laser can adopt any mode size, as dictated by the aperture. This results in nearly identically high Q factors for many transverse modes at each aperture size (FIG. 2c). Hence, spatial filtering outside a laser is much less efficient than filtering inside a degenerate cavity.

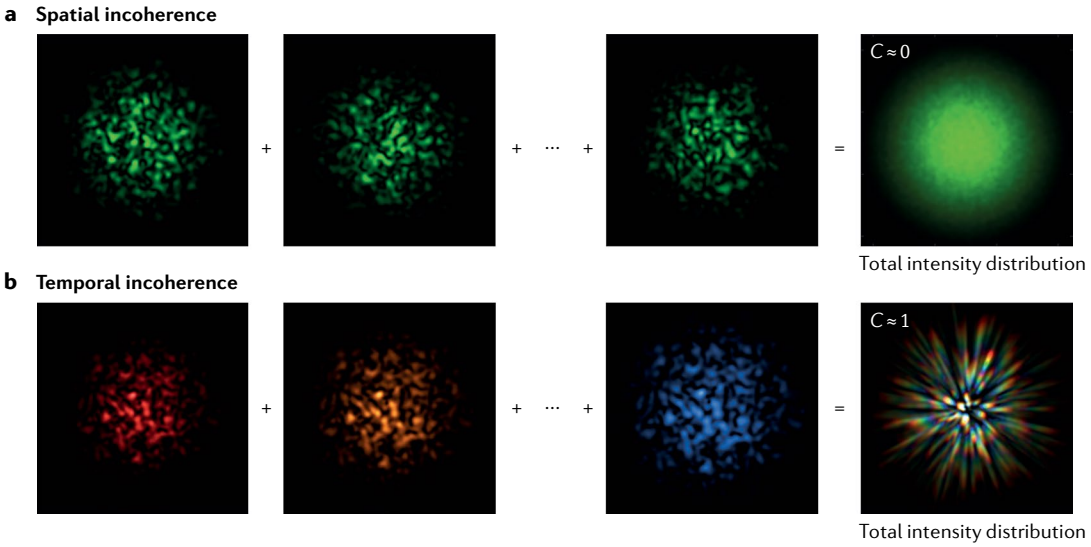

Fig. 1 | **Simulations of speckle suppression with low spatial coherence or low temporal coherence. a** | For low spatial coherence, independent spatial modes of light are mutually incoherent. Each mode generates a distinct speckle pattern. The intensity sum of these patterns reduces the speckle contrast (*C*). **b** | Low temporal coherence emission from broadband light source in a single spatial mode. Each wavelength generates a speckle pattern that is only marginally different from the others. The wavelength difference results only in a radial rescaling of the generated speckle pattern and leads to a limited reduction in speckle contrast. Adapted with permission from REF.[62], copyrighted by the American Physical Society.

Spatial coherence properties can be further manipulated in a degenerate cavity laser by using more sophisticated intracavity spatial filters[16]. For example, a variable slit enables independent control of the spatial coherence length on one axis without affecting the orthogonal axis. Alternatively, two pinholes, an annular band or an array of circular holes can generate cosine, Bessel or comb-like spatial coherence functions, respectively. In principle, arbitrary spatial coherence functions can be obtained with a degenerate laser without losing power.

Multimode fibre amplifiers. In fibre lasers, the gain medium is in the core of a long fibre, which is typically doped with Er or Yb ions. It is difficult to integrate it into a degenerate cavity, and so a different approach for reducing the spatial coherence is required. This can be done by increasing the number of guided modes, that is, modes that are confined to the gain core. A recently developed multimode fibre with an extra-large mode area (XLMA) gain core supports numerous guided modes (FIG. 3a). However, the lower-order modes are more tightly confined within the gain core, thereby experiencing stronger amplification than the higher-order modes. Hence, the lower-order modes tend to deplete the gain and suppress the higher-order modes. Consequently, equalizing modal gain and reducing modal competition are necessary to obtain amplification of many guided modes. A simple way to equalize the modal gain is to introduce mode coupling. For example, fibre bending and twisting or imperfections such as fluctuations of the refractive index and variations of the fibre cross section cause random coupling among the modes and thus reduce mode-dependent gain.

One method for reducing modal competition is to operate in the regime of amplified spontaneous emission (ASE). This is achieved by cleaving the fibre end facets at an angle to minimize feedback for lasing[12]. A rare-earth-doped XLMA fibre ASE source has not only low spatial coherence (FIG. 3b) but also low temporal coherence owing to its broad emission spectrum (FIG. 3c). In addition, the output beam is highly directional, with the divergence angle dictated by the small numerical aperture of the fibre. The spatial profile of the output beam is smooth (FIG. 3d) even though it contains many spatial modes. For comparison, semiconductor-based superluminescent diodes have relatively high spatial coherence (FIG. 3e), because they are based on 1D waveguides that have far fewer transverse modes and much weaker mode mixing than XLMA fibres[17].

Wave-chaotic microcavity lasers. In the two lasers discussed above, the lasing modes could be separated into longitudinal and transverse modes, and spatial coherence was reduced by increasing the number of transverse modes. A more dramatic way of reducing spatial coherence is by eliminating this separability so that all lasing modes have distinct emission profiles. In this way, all lasing modes contribute to the reduction in spatial coherence unless they are phase locked. To this end, a fundamental change in the laser cavity geometry is necessary.

Resonators with separable geometry, such as the stable resonators discussed in the introduction or circular cavities (FIG. 4a–c), are integrable. In other words, the wave equation can be solved analytically, and the resonant modes are labelled with sets of quantization numbers corresponding to the coordinate axes, for example, radial and azimuthal indices in the case of a circle. In addition, separable cavities feature integrable classical ray dynamics: a small deviation of the initial conditions

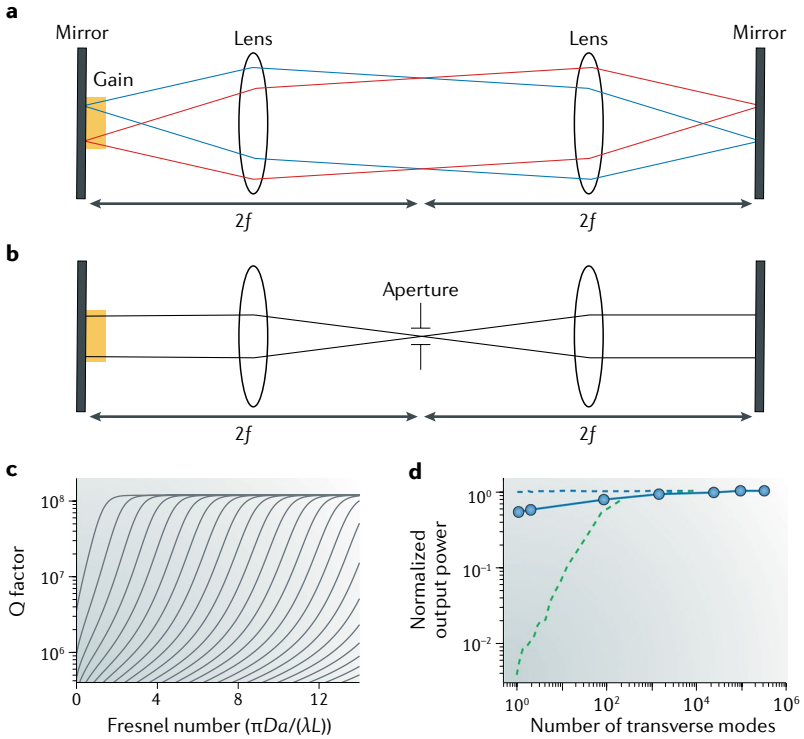

Fig. 2 | **Degenerate cavity lasers with tunable spatial coherence. a** | Schematic of a degenerate laser cavity in a self-imaging configuration. Light emitted from any point in the gain medium is imaged back to itself after one round trip. A large number of independent transverse modes lase simultaneously and independently to produce low spatial coherence. **b** | Inserting an aperture in the mutual focal plane of the two lenses yields a single transverse mode emitting with high spatial coherence. **c** | Calculated cavity Q factors of the 24 lowest-order transverse modes as a function of the Fresnel number, in which the aperture diameter a is varied, the length of the degenerate cavity with an output coupler of 90% reflectivity is $L = 1$ m, the diameter of the circular cross section of the gain medium is $D = 1$ cm and the wavelength $\lambda = 1{,}064$ nm. As the aperture diameter increases, additional transverse modes appear, and their Q factors rise quickly to approach the value of existing modes. **d** | Measured output power as a function of the number of transverse modes in the degenerate cavity (solid blue line) compared with the predicted output power for a degenerate cavity laser (dashed blue line) and a stable hemispherical cavity (dashed green line). The measurement was done with a degenerate cavity comprising two lenses with a focal length $f = 25$ cm and an Nd:YAG (neodymium-doped yttrium aluminium garnet) crystal of 11 cm in length and 0.95 cm in diameter. Panels **a** and **b** are adapted with permission from REF.[76], OSA. Panel **d** is adapted with permission from REF.[15], OSA.

of two trajectories leads to a divergence that scales at most linearly with time.

Cavities with non-separable geometries, by contrast, can exhibit partially or completely chaotic ray dynamics[18,19], in which small deviations of the initial conditions lead to a divergence of trajectories that scales exponentially with time. One example is a circular cavity with a section removed along a straight cut (FIG. 4d), which leads to fully chaotic ray dynamics[20]. Because its shape resembles the letter D, it is called a D-cavity.

Regardless of whether ray dynamics are integrable or chaotic, passive cavity modes do not exhibit exponential dependence on the initial conditions, because the modes are solutions to the linear Helmholtz equation. However, the classical ray dynamics manifests in the mode properties according to the principle of ray–wave correspondence[21]. Cavities with chaotic ray dynamics, called wave chaotic, show qualitative differences compared with integrable ones. The modes of wave-chaotic cavities cannot be labelled with sets of quantization numbers because their geometry is non-separable, and the modes are generally non-degenerate[18]. Moreover, the field distributions of the modes feature irregular patterns of wavelength-sized grains that can spread over the whole cavity, as in the classical trajectories (FIG. 4e,f); thus, each mode has a distinct emission field profile. By contrast, modes of integrable cavities feature very regular field patterns (FIG. 4b,c) that can have identical emission profiles if one of their quantization numbers matches. One important feature of the dielectric circle resonator is the existence of whispering gallery modes (WGMs) with extremely high Q factors that correspond to trajectories near the circumference confined by total internal reflection (FIG. 4a).

The ray–wave correspondence also affects lasing dynamics. Lasing in a circle is dominated by WGMs because their thresholds are very low. The number of lasing modes is limited by the strong gain competition of the WGMs, which is caused by their localization near the boundary. By contrast, a D-shaped dielectric disk supports a large number of chaotic lasing modes that have almost identical thresholds thanks to their relatively high but similar Q factors[22]. Because their field distributions are typically widely spread over the cavity, their competition for gain is much weaker than that of WGMs. Consequently, many more modes can lase simultaneously in a D-cavity than in a circular cavity. All lasing modes have distinct emission profiles and thus contribute to the reduction in spatial coherence. Optimization of the position of the straight cut in the D-cavity allows the modes to spread more uniformly across the cavity to minimize their gain competition, and the differences in their lasing thresholds is further reduced. The maximum number of lasing modes in the D-cavity is attained when the cut is half the radius from the centre[22].

Not all wave-chaotic cavities are necessarily well suited for highly multimode lasing. In addition to spatially extended modes, they can exhibit scar modes that are localized on unstable periodic orbits[19,23]. If the scar modes have higher Q factors than those of the chaotic modes, they dominate lasing, and their strong competition for gain (due to large spatial overlap) will limit the number of lasing modes. One advantage of the D-cavity is that all scar modes have low Q factors because the angles of incidence of the underlying periodic orbits are below the critical angle for total internal reflection.

A disadvantage of the D-cavity laser for practical applications is that its emission is nondirectional because its modes consist of plane wave components travelling in all possible directions, similar to the classical ray trajectories. Directional emission from a wave-chaotic cavity can be obtained by modifying the cavity geometry so that long-lived ray trajectories reach the critical angle of total internal reflection only at certain parts of the boundary and therefore refract towards particular directions[19,24]. Creating a wave-chaotic cavity that combines low spatial coherence with directional emission is a future challenge.

Random lasers. In a wave-chaotic cavity, light is confined by reflection at the cavity boundary, and so the cavity shape determines the spatial and spectral properties of the resonant modes. Alternatively, light scattering

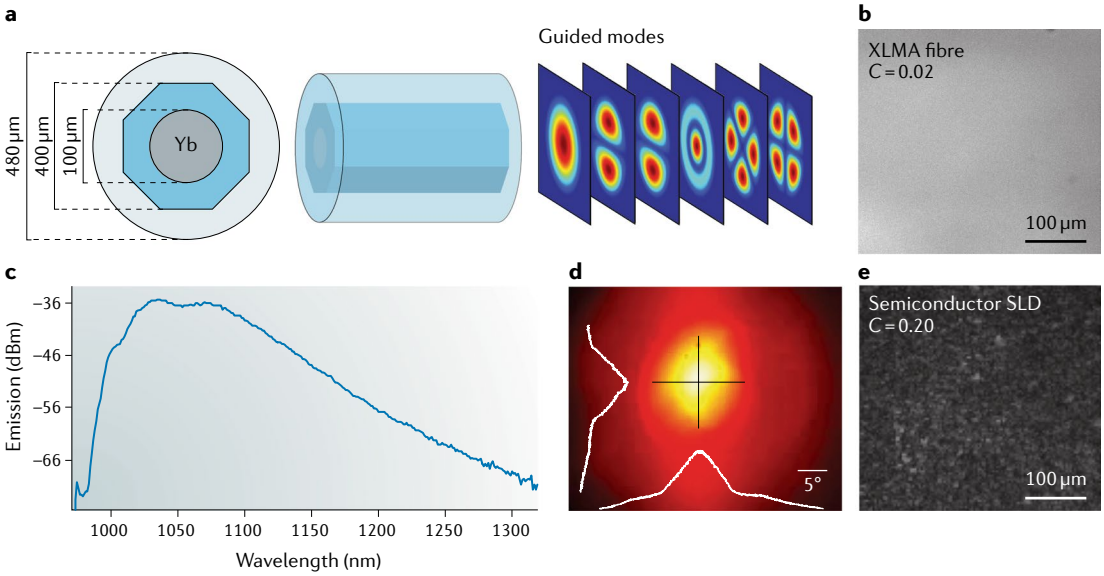

Fig. 3 | **Fibre laser with low spatial coherence. a** | Cross section of the Yb-doped extra-large mode area (XLMA) fibre (left) and multiple guided modes (right). The 100 µm diameter Yb-doped core is surrounded by a 400 µm diameter octagonal cladding and a 480 µm diameter outer cladding. **b** | Image of transmission through a diffuser illuminated by amplified spontaneous emission (ASE) from the XLMA fibre, which efficiently suppresses speckle with a measured contrast of $C = 0.02$. **c** | Measured emission spectrum of the fibre ASE source. **d** | Spatial profile of the output beam from the fibre ASE source with a divergence angle less than 6°. **e** | Illuminating the same diffuser as in panel **b** with ASE from a multimode superluminescent diode (SLD) leads to a speckle contrast of $C = 0.2$. Adapted with permission from REF.[12], OSA.

induced by structural disorder can trap light and provide feedback for lasing even in the absence of a well-defined cavity[25–27]. In a gain medium that contains numerous scattering centres, spontaneously emitted photons are scattered many times and undergo a random walk (FIG. 5a). Multiple scattering centres increase the path length of photons travelling in the gain medium, and this increase in path length enhances the stimulated emission of photons that amplifies light[28,29]. Furthermore, the scattered waves may return to spatial positions they have visited before, providing coherent feedback and enabling laser oscillation[30–32]. Such a laser is called a random laser. It has been implemented in various material systems, including powders[33], polycrystalline films[34], colloids[35], polymers[36], optical fibres[37] and organic materials[38]. The lasing frequencies range from ultraviolet[39] and visible[40] to infrared[41] and terahertz[42]. Although lasing is realized in both strong and weak scattering systems, the lasing threshold is lower when scattering is stronger[43].

Most random lasers operate in the highly multimode regime. Individual lasing modes, formed by the interference of scattered waves, have distinct frequencies and spatial structures[44,45], which result from the non-separable geometry of the system, as in the case of wave-chaotic cavities. For example, the spatial field intensity distribution for a lasing mode in a 2D diffusive medium[46] fluctuates spatially on the wavelength scale, and the mode spreads more or less uniformly over the entire system (FIG. 5b). When a large number of such modes lase simultaneously with uncorrelated phases, their distinct wavefronts combine incoherently to produce emission with low spatial coherence[47]. The random laser directly generates light of low spatial coherence, in contrast to the conventional approach of reducing spatial coherence of light from a coherent laser using mechanisms such as spinning diffusers. In the conventional approach, uncorrelated speckle patterns are sequentially formed by a time-varying system (the spinning diffuser) outside the laser cavity; in the random laser, scatterers are directly incorporated into the gain medium to simultaneously generate many independent speckle patterns, one from each lasing mode.

The number of random lasing modes increases with the scattering strength[25]. As the transport mean free path approaches the emission wavelength, the number of lasing modes rises quickly[43]. Because stronger scattering leads to tighter confinement of random lasing modes, the spatial overlap of the modes is reduced, and their competition for gain becomes weaker. Hence, the spatial coherence of random laser emission can be tuned by varying the density of scatterers (FIG. 5c–h). Furthermore, the pump beam diameter is typically smaller than the sample size, and so increasing the excitation pump beam size allows more modes to lase[33]. Thus, the spatial coherence can also be tuned by changing the pump beam profile[48].

Large-aperture VCSELs. In the lasers discussed above, the spatial coherence of laser emission was tailored by modifying the cavity geometry or internal structure. These cavity-based approaches are static and aim to manipulate the steady state of lasing. Here, we describe a dynamic approach that relies on pulsed pumping. The aim is to disrupt the operation of lasing so that the steady state is not reached. Instead, the laser operates in a transient regime, in which spatial coherence does not build up. This approach can be implemented with large-aperture VCSELs. The cavity length is on the order of the

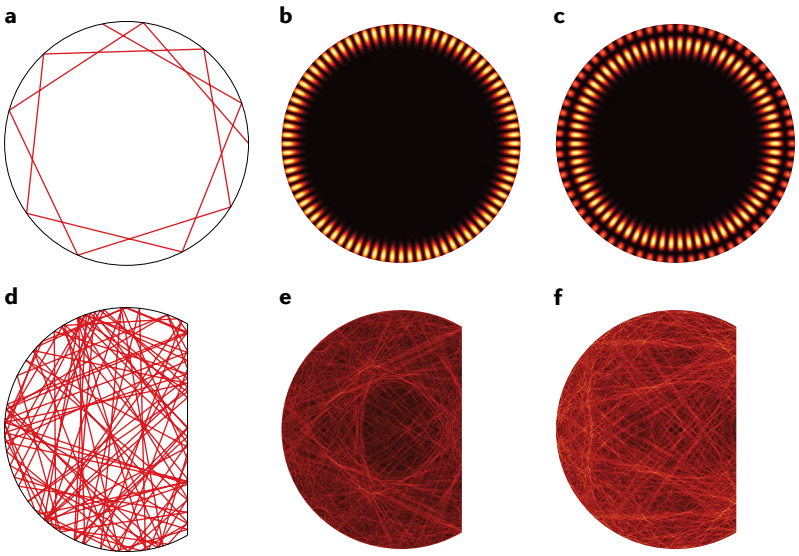

Fig. 4 | **Calculated resonant modes in 2D microcavities with regular or chaotic ray dynamics. a** | A circular cavity containing a whispering gallery trajectory that stays close to the cavity boundary. **b,c** | Spatial intensity distributions of two whispering gallery modes that are confined to the boundary of a circular dielectric disk. **d** | A typical ray trajectory in a D-shaped cavity spreads over the entire cavity because of the chaotic ray dynamics. **e,f** | Spatial intensity distributions of two resonances in a D-shaped dielectric disk that displays an irregular, fine-grained structure.

emission wavelength, and so only one or at most a few longitudinal modes exist[49]. However, many more transverse modes exist, because the diameter of the aperture is much larger than the wavelength. The aperture shape is typically circular, but when it is deformed, the onset of wave-dynamical chaos is observed[50,51].

When a large-aperture VCSEL is driven by a current pulse, spatially inhomogeneous heating of the device forms a thermal lens, which leads to an increase in the time to build up modes[52]. In addition, during the current pulse, the cavity is constantly expanding and remains non-stationary, causing a strong thermal chirp. Consequently, the cavity modes cannot build up because the cavity environment changes faster than the mode build-up time, and stimulated emission is generated from small, independent, local 'coherence islands'. The VCSEL operates in a nonmodal state, which is a superposition of these islands[53]. The spatial coherence of emission is low, resulting in the formation of a Gaussian far-field intensity distribution.

By tuning the pump pulse duration and amplitude, the degree of spatial coherence can be varied[54,55]. When a strong thermal lens is established by a constant bias current, a low-amplitude current pulse with a 50% duty cycle can create a thermal chirp to break up the global cavity modes.

In addition to spatial coherence control, a current sweep operation scheme to reduce the temporal coherence of VCSELs has been developed[56,57]. In the scheme, a rapidly modulated pump current is applied, which leads to reduced temporal coherence because thermal effects within the small cavity broaden the effective spectrum. One advantage of VCSELs for this scheme is that their small gain volume allows rapid thermal changes to produce spectral effects on a short timescale.

Comparison of strategies and implementations. Each of the strategies and implementations for reducing spatial coherence has advantages and disadvantages. The simplest way to reduce spatial coherence is to form an array of independent lasers, for instance, a 1D array of edge-emitting laser diodes or a 2D array of VCSELs. These lasers must be sufficiently far apart to avoid coupling; thus, the total array size and the fabrication cost increase with the number of lasers. To increase the total number as well as the area density of lasers, it is easier to incorporate them all in a single cavity, such as a degenerate cavity. An additional advantage of degenerate cavities is that the number of transverse lasing modes can be readily controlled to tune the spatial coherence with little power change. Moreover, a nonlinear crystal can be inserted in a degenerate cavity to obtain intracavity frequency doubling[58]. The number of transverse modes at the second harmonic frequency is even larger than that at the fundamental frequency, and thus laser emission of low spatial coherence is produced at both frequencies. However, degenerate cavity lasers are relatively bulky and require careful alignment. Multimode fibre amplifiers are more robust and compact than degenerate cavity lasers and have high efficiency, and as ASE sources, they exhibit both low spatial and low temporal coherence. However, tuning their coherence is relatively difficult.

Wave-chaotic microcavity lasers and random lasers are different from conventional lasers but are similar to each other in many ways. Both systems have a non-separable geometry, owing to an asymmetric cavity shape or random refractive index variations, respectively. Most wave-chaotic cavities have 2D geometries and are relatively easy to produce with standard microfabrication techniques. Random lasers are more flexible and have been realized in 1D, 2D and 3D geometries. Both random and wave-chaotic lasers are compact and robust, and the number of lasing modes can be changed by spatial modulation of the pump[59–61], thereby enabling spatial coherence control[48]. However, for these lasers, it remains a challenge to combine directional emission with low spatial coherence.

Temporal modulation of the pump can also greatly reduce the spatial coherence of laser emission and provides a simple method for generating partially coherent, directional beams from large-aperture VCSELs. However, during parts of a pump modulation period, there is either no lasing emission or emission occurs with high spatial coherence. The degree of spatial coherence can be periodically modulated at a repetition rate as high as 500 kHz (REF.[54]). In conclusion, which of the above laser systems provides the most suitable low-spatial-coherence light source depends on the desired application.

Applications of complex lasers

Many high-speed imaging applications require short detection times, but it is difficult to simultaneously achieve low speckle contrast and a short exposure time of the detector. For example, consider a laser with N spatial modes that are frequency degenerate. Each mode has a linewidth of $\delta\omega$, corresponding to a coherence time $\tau_c = 1/\delta\omega$. When illuminating a static scattering

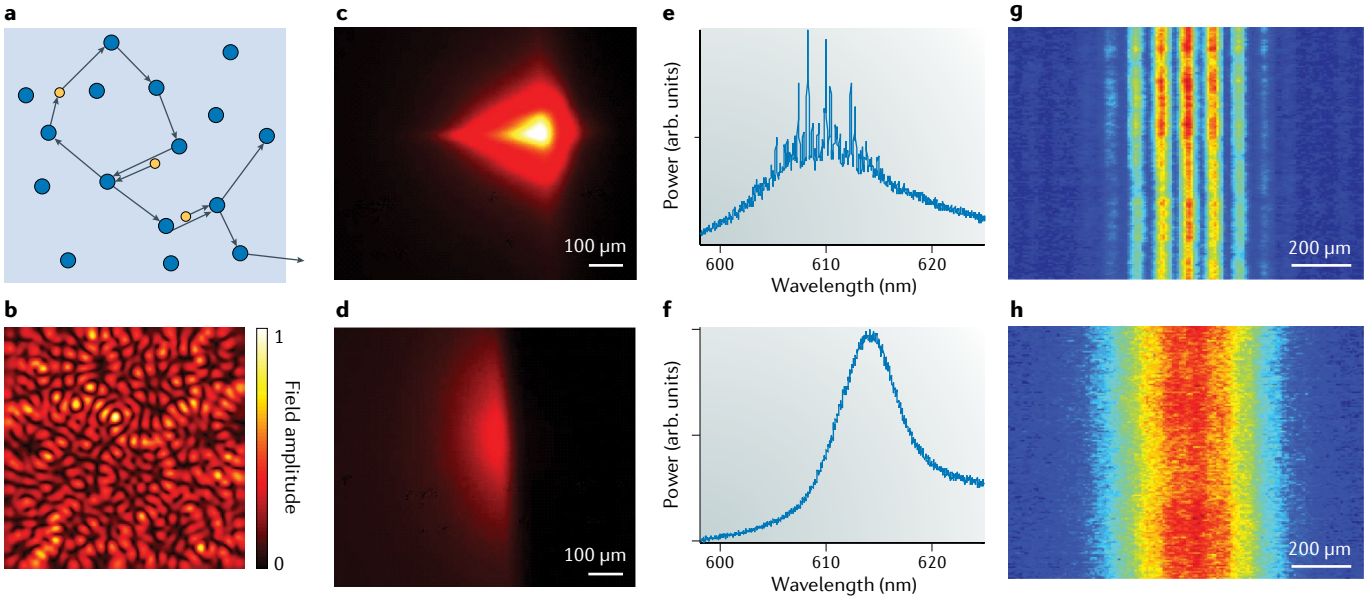

Fig. 5 | **Spatial coherence of random lasers.** Schematic of multiple scattering centres and stimulated emission of photons in a random medium (panel **a**). The black circles denote scattering centres, and the orange dots are excited atoms. Calculated spatial field amplitude distribution of a lasing mode in a 2D ($5 \times 5\ \mu m^2$) random array of dielectric cylinders in air (panel **b**). The cylinders have a radius of 60 nm, refractive index of 1.25 and filling fraction of 40%. Experimental data for random lasers (colloidal solution with dye molecules pumped optically) in the weak (panels **c,e,g**) and strong (panels **d,f,h**) scattering regimes. Side-view images of the excitation volume in a Rhodamine 640 solution with polystyrene spheres (panels **c,d**). The scattering mean free path is 50 μm in the strong scattering regime and 500 μm in the weak scattering regime. Normalized emission spectra for a single pump pulse (at a wavelength of 532 nm) with a pulse energy that is twice the lasing threshold (panels **e,f**). The number of lasing modes is higher in the strong scattering regime, resulting in a smooth spectrum. Far-field patterns of random laser emission through a double slit (panels **g,h**). The interference fringes with high contrast in panel **g** indicate that the random laser in the weak scattering regime has high spatial coherence, whereas the lack of interference fringes in panel **h** reveals that the random laser in the strong scattering regime has low spatial coherence. Panel **b** is adapted with permission from REF.[46], copyrighted by the American Physical Society. Panels **c**–**h** are adapted with permission from REF.[48], OSA.

medium, each mode generates a distinct speckle pattern. If the exposure time is less than the coherence time, all modes are phase coherent with each other, and so their scattered fields are added together coherently to form a new speckle pattern with unity contrast. However, if the exposure time is much longer than the coherence time, the modes are mutually incoherent, and their speckle patterns combine to yield an increase in intensity, lowering the contrast to $1/\sqrt{N}$.

If the spatial modes are non-degenerate, their frequency difference accelerates the loss of coherence. Assuming the frequency spacing $\Delta\omega$ between spatial modes exceeds their linewidth $\delta\omega$, they will be mutually incoherent for an exposure time longer than $1/\Delta\omega$. Therefore, the spectral repulsion of lasing modes in a random medium[30] or a wave-chaotic cavity[18] shortens the exposure time that is needed for speckle suppression.

In a degenerate cavity[62], the frequency spacing $\Delta\omega_l$ between longitudinal modes is usually much larger than the spacing $\Delta\omega_t$ between the transverse modes. On the short timescale of $1/\Delta\omega_l$, all transverse modes with identical longitudinal mode indices remain phase coherent, and they interfere to generate a speckle pattern of unity contrast. Each longitudinal mode group produces a distinct speckle pattern, because the phase differences between modes in each group are different. These speckle patterns are mutually incoherent, and an intensity sum of all M independent speckle patterns, where M is the number of longitudinal modes, reduces the speckle contrast to $1/\sqrt{M}$, assuming that M is less than the number of transverse modes N. On the long timescale of $1/\Delta\omega_t$, all transverse modes can combine incoherently to give a speckle contrast of $1/\sqrt{N}$.

Because the spatial coherence of a laser is determined by the number of transverse lasing modes, it can be controlled by the geometry and/or internal structure of the cavity. Generally, the schemes for reducing the spatial coherence, as described in the previous section, are applicable to a variety of lasers, which can operate at different wavelengths and with different gain materials. An alternative scheme for lowering the spatial coherence, which is applicable to broadband illumination sources, is to transform temporal incoherence to spatial incoherence via spectral or spatial dispersion[63,64].

In the following, we describe several applications for which lasers with low and/or tunable spatial coherence are needed. Several specific examples with relevant and practical parameters are presented.

Speckle-free imaging. The ability of a laser with low spatial coherence to suppress speckle noise directly leads to improved image quality, especially when imaging in a scattering environment[65]. This can be seen by comparing images obtained by using different illumination

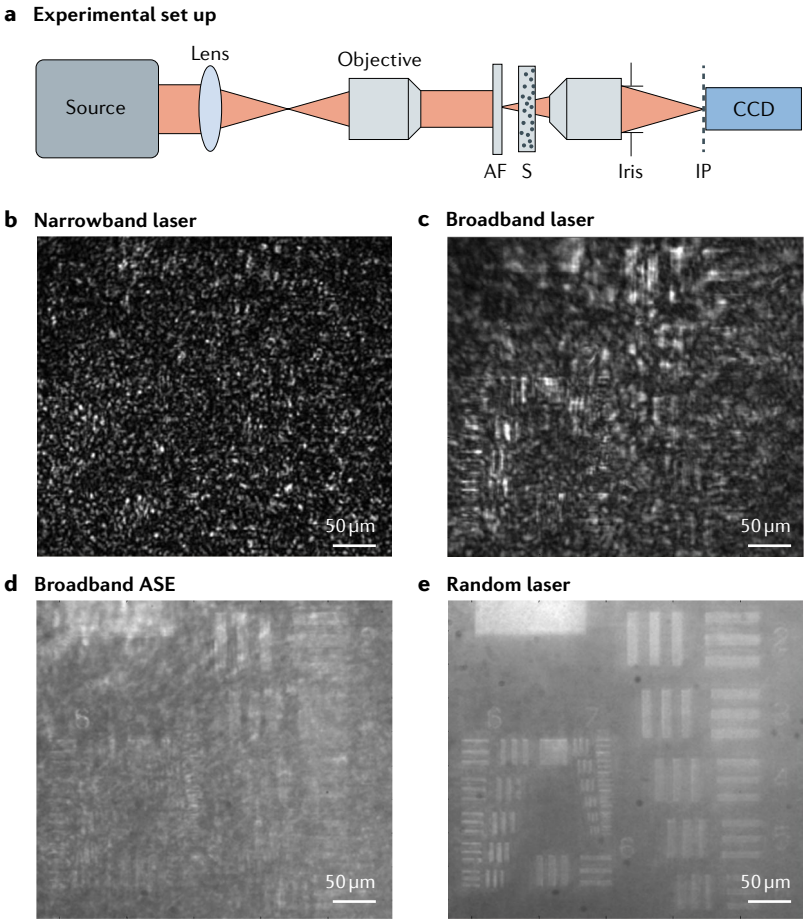

Fig. 6 | **Full-field imaging through a scattering medium. a** | Schematic of the experimental setup used to image a US Air Force resolution test chart (AF) through a thin static scattering film (S). The scattering film is placed between the test chart and the objective, which images the test chart on the image plane (IP) of the charge-coupled device (CCD) camera. **b** | Image made with a narrowband laser (He:Ne laser at 633 nm). **c** | Image made with a broadband laser (mode-locked 200 fs Ti:Sapph laser). **d** | Image made with an amplified spontaneous emission (ASE) source (Rhodamine 640 dye solution). **e** | Image made with a random laser (Rhodamine 640 dye solution with polystyrene scatterers). The first three sources have high spatial coherence, resulting in notable speckle noise, and the last one has low spatial coherence, yielding a speckle-free image. Adapted from REF.[65], Springer Nature Limited.

sources for full-field imaging of a US Air Force test chart through a static scattering medium (FIG. 6a). Under spatially coherent illumination with a conventional narrowband laser, interference among scattered photons produces strong speckle noise that corrupts the image beyond recognition (FIG. 6b). The image is corrupted even when using a broadband laser (FIG. 6c) or an ASE source (FIG. 6d), which have relatively low temporal coherence. By contrast, when illuminating with a random laser of low spatial coherence, there is little, if any, interference between scattered photons, leading to a uniform background level (FIG. 6e). Although the scattered photons increase the background level and lower the image contrast, the features of the object remain clearly visible. In a different experiment, it was shown that even a narrowband random laser, which has high temporal coherence, could provide speckle-free illumination for full-field imaging[66].

In the case of fluorescence imaging, in which the fluorescence itself is spatially incoherent and does not produce speckle, coherent artefacts must still be dealt with. This is because the pump light is often a coherent laser beam. The coherent artefacts of the pump generate spatially non-uniform excitation of the fluorescence, which leads to artificial variations in the measured intensity. This problem has been overcome by using intracavity frequency doubling of a solid-state degenerate laser to generate emission suitable for exciting fluorescence without coherent artefacts[58].

The speckle noise depends not only on the coherence properties of the illumination source but also on the imaging optics, including factors such as the ratio of the numerical aperture for observation to the numerical aperture for illumination[67]. Accordingly, the required degree of spatial incoherence of an illumination source to suppress speckle noise depends on various parameters of a specific application, such as the amount of scattering or the imaging resolution. For example, a multimode laser could be designed to provide sufficiently low spatial coherence to enable speckle suppression while maintaining relatively high power per mode, compared with existing spatially incoherent sources such as lamps and LEDs. Typically, approximately 1,000 spatial modes are sufficient to suppress speckles below the level observable by humans[10,11]. Lamps and LEDs emit photons into a far larger number of modes than this and thus have lower brightness than would be optimal. A quantitative measure of the source brightness is the number of photons per coherence volume, known as the photon degeneracy parameter δ (REF.[3]). It is proportional to the spectral radiance, which is a radiometric measure of the flux in a unit frequency bandwidth that passes through a unit area and into a unit solid angle. The values of δ for random lasers and chaotic microcavity lasers are several orders of magnitude higher than those of lamps and LEDs[22]. The greatly improved photon degeneracy allows much shorter exposure times and much higher speed for the full-field imaging of transient processes. For example, a random laser can be triggered to produce a short illumination flash at a well-defined delay time, thereby providing uniform, speckle-free background illumination[68]. This procedure enables time-resolved microscopy with an exposure time as short as 10 ns (REF.[68]).

Spatial coherence gating. In addition to speckle-free imaging, highly multimode lasers can provide spatial coherence gating for interferometric detection, enabling parallel confocal image acquisition. In general, confocal microscopy combines high spatial resolution, high contrast and optical sectioning[6]. Traditionally, confocal microscopy relies on raster scanning, which limits the speed of image acquisition[69]. The process can be sped up by parallelization; commonly, this is done using an array of spatially separated pinholes[70], which must be sufficiently separated to prevent crosstalk. Parallelization can also be achieved by combining interferometric detection with spatial coherence gating[71]. This approach uses virtual pinholes, which are formed by each spatial mode. Unlike physical pinholes, the virtual pinholes do

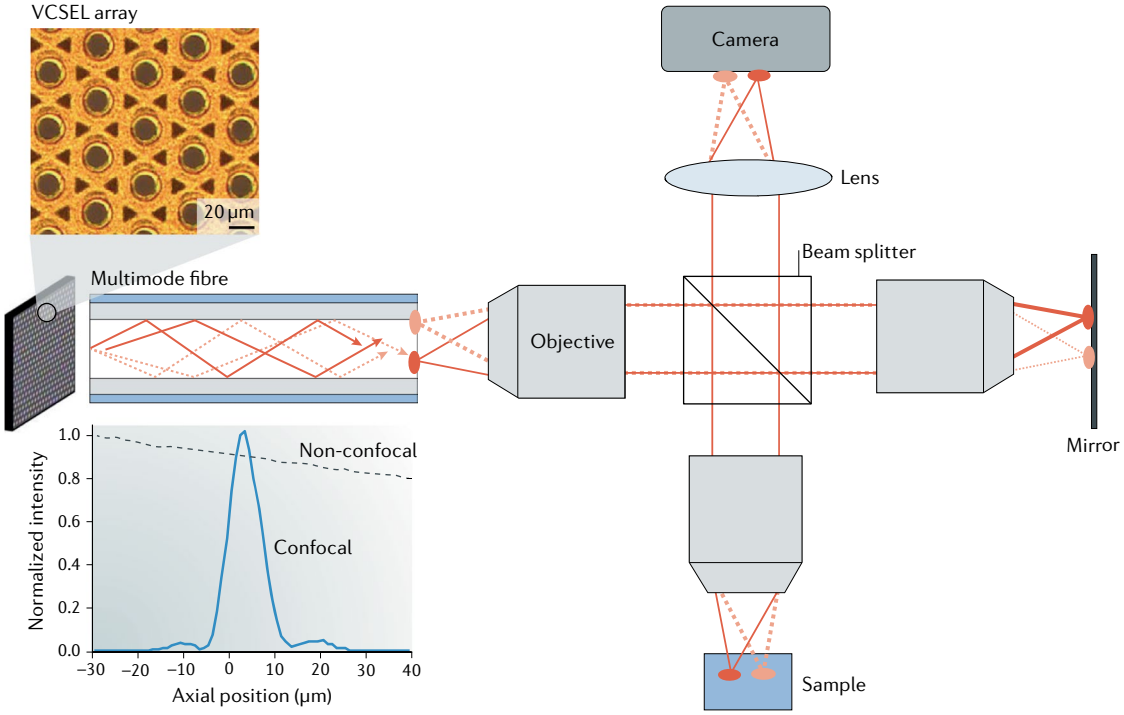

Fig. 7 | **Full-field interferometric confocal microscope.** The vertical-cavity surface-emitting laser (VCSEL) array is coupled to a multimode fibre, which mixes mutually incoherent emission from 1,200 independent lasers and provides a uniform low-spatial-coherence illumination on the sample. Light reflected from the sample combines with that from the mirror at the beam splitter, and the resulting interference patterns are recorded by the camera. The upper inset shows part of the VCSEL array, in which each circle of ~20 μm diameter represents one emitter. The lower inset shows the axial point spread function (blue solid line), the width of which gives the axial resolution of ~8 μm. The black dotted line represents the conventional wide-field microscope, in which the recorded intensity decays slowly with defocus. Adapted with permission from REF.[72], OSA.

not require physical separation to avoid crosstalk. This enables parallel acquisition of an entire en face plane in a single snapshot, without requiring scanning. Although this approach is not suitable for fluorescence imaging, it holds potential for constructing high-speed, large-area reflectance imaging systems that feature confocal resolution and sectioning. However, the microscopes require light sources that have not only low spatial coherence but also sufficient power per mode. This requirement is met by lasers with low spatial coherence.

A further advantage of using laser sources with low spatial coherence is that the number of virtual pinholes can be much larger than the number of simultaneous independent spatial lasing modes. For example, an interferometric confocal microscope, which uses an array of 1,200 VCSELs coupled to a multimode fibre, has been constructed[72] (FIG. 7). The microscope performs interferometric detection, using an off-axis holography technique, and can therefore acquire, in parallel, image information from 18,000 continuous virtual pinholes. The number of virtual pinholes is set by the number of resolvable elements provided by the microscope objective, a number that is determined by the field of view and the point spread function. The number of emitters in the VCSEL array does not limit the number of virtual pinholes, because the lasers are combined to eliminate crosstalk using averaging and do not serve as independent imaging channels.

Interferometric detection of fields that have low spatial coherence has another advantage: it yields a coherent signal that is inherently confocal in the transverse plane and along the axial dimension, which is beneficial for both transverse and axial resolution. The microscope described in REF.[72] and FIG. 7 provides en face images with a 210 μm × 280 μm field of view, ~2 μm transverse resolution and ~8 μm axial resolution in a single shot. The high photon degeneracy allows the integration times to be as short as 100 μs and enables a 2D frame rate above 1 kHz. Interferometric detection also recovers the phase of the optical field, which can be used to estimate the height of sub-resolution axial features[73]. Ultrahigh-speed, full-field holographic confocal microscopy is used for in vivo quantitative studies of microscale physiology[74].

Bimodal imaging. Whereas a speckle-free wide-field image provides structural information about an object, the speckle formed by random scattering of coherent light carries additional information about the object's motion. For example, dynamic scatterers in a biological sample, such as moving blood cells, induce time-dependent phase shifts in the scattered light, causing temporal changes in the speckle pattern. Such changes can be used to map blood flow in living tissues by a technique called laser speckle-contrast imaging[75].

Anatomical and functional information about living tissue can be acquired by bimodal imaging. For instance,

laser speckle-contrast microscopy that maps neural blood flow can be combined with intrinsic signal optical imaging that monitors tissue oxygenation. This combination has been achieved using two separate illumination sources — a laser and an LED — and switching rapidly between them[56]. However, lasers and LEDs typically have very different beam divergence angles and power densities, and separate optical setups are necessary for beam collimation and power adjustment to ensure that the illumination area and the light intensity do not change much when switching between sources. Therefore, a single illumination source with tunable spatial coherence but constant power and beam size would be advantageous for such applications. It could be possible to increase the spatial coherence of an LED by spatial filtering, but then, the power would be greatly reduced. A better, and probably the best, scenario is to tune the spatial coherence of a laser, such as a degenerate cavity laser, with little power loss[15,16].

An electrically pumped semiconductor-based degenerate vertical-external-cavity surface-emitting laser with continuous wave emission has been developed for imaging embryo heart function in *Xenopus*, an important model organism for studying heart disease[76]. The spatial coherence of the laser emission was switched between low and high: low-spatial-coherence illumination enables high-speed (100 frames per second) speckle-free imaging of the dynamic heart structure, and high-spatial-coherence illumination enables laser speckle-contrast imaging of blood flow.

Laser wavefront shaping. A unique feature of the degenerate cavity laser is that it can produce arbitrary output beam profiles. Beam shaping is a key technology used to apply high-power lasers to materials processing and device fabrication[77]. Traditionally, external shaping of a laser beam (outside of the laser cavity) to a desired transverse profile has been implemented with a variety of elements and techniques, including diffractive optical elements, free-form optics and digital holography with spatial light modulators. For example, an aspherical or diffractive element can transform a Gaussian intensity profile of a single-mode laser beam to a flat-top beam. However, a multimode degenerate cavity laser can directly generate an output beam with a flat-top profile[58]. This is because the degenerate cavity laser has the unique feature that it can support a large number of transverse modes with almost identical frequencies but different spatial wavefronts. It is possible to superimpose these modes to produce arbitrary output beam profiles by using intracavity elements.

In general, the profiles of light beams vary as they propagate owing to diffraction. These variations of the beam profiles can be controlled by manipulating spatial coherence[78]. In the 4*f* degenerate cavity laser (FIG. 2a), direct access to both the real and Fourier spaces of the lasing modes enables simultaneous control of the beam profile and the spatial coherence. Shaped beams with tailored spatial coherence can be obtained by inserting an amplitude mask near one of the mirrors and a Fourier mask in the mutual focal plane of the two lenses[79]. If the Fourier mask is a circular aperture, decreasing the aperture diameter blocks the large transverse wave vector components; thus, the output beam experiences less diffraction upon propagation, but the minimal feature size of its spatial profile is increased. It is possible to produce a shaped beam that is propagation invariant by using an annular aperture Fourier mask (FIG. 8a) to obtain a Bessel spatial coherence function of

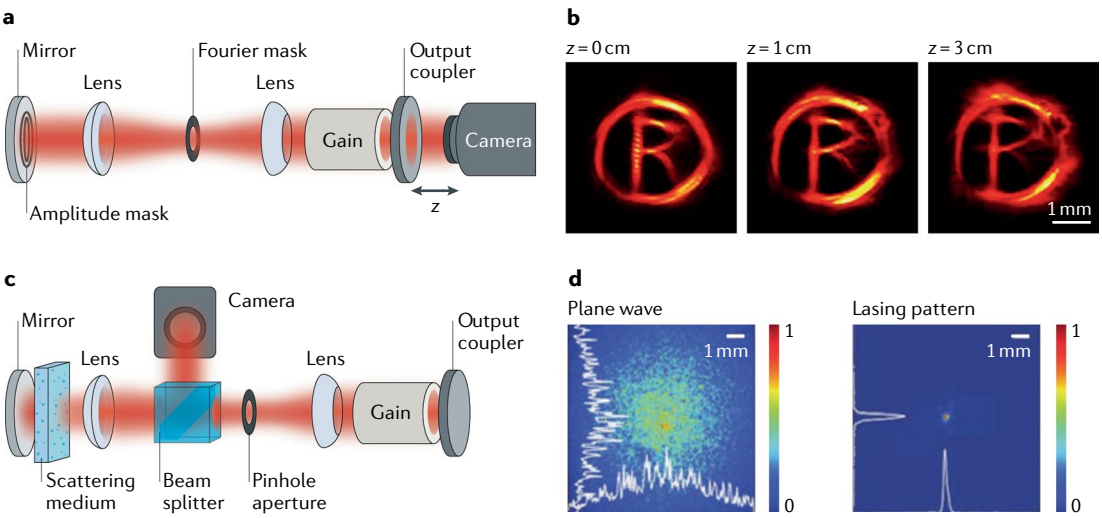

Fig. 8 | **Laser wavefront shaping within a degenerate cavity laser.** Generation of propagation-invariant beams in a degenerate laser cavity. An amplitude mask is placed close to the back mirror, and an annular ring is placed in the mutual focal plane of the two lenses (panel **a**). The resulting output beam maintains its transverse profile for a relatively long propagation distance *z* from 0 cm to 3 cm (panel **b**). Focusing light through a scattering medium (panel **c**). A scattering medium is placed inside the degenerate cavity near the back mirror, and a small pinhole aperture is placed at the Fourier plane to ensure focusing of the laser light. Intensity distribution at the plane of the pinhole aperture (shown in the right panel), recorded by the camera with a beam splitter, compared with the intensity distribution obtained by focusing light through a scattering medium (outside the cavity) by wavefront shaping with a spatial light modulator (shown in the left panel; panel **d**). Panels **a** and **b** are adapted with permission from REF.[79], OSA. Panel **d** is adapted from REF.[81], Springer Nature Limited.

the emission. The output beam, regardless of its transverse profile (which is set by an intracavity amplitude mask), can propagate over a relatively long distance with minimal diffraction (FIG. 8b). A geometric phase metasurface element can also be incorporated into a degenerate cavity laser as an output coupler, enabling efficient generation of spin-dependent twisted light beams with different topologies[80].

In addition to shaping the output beam, wavefront shaping can be used to control light so that it can be focused through a random scattering medium. In one experiment, a random scattering medium was placed inside a degenerate cavity laser[81]. The light scattered by a rapidly varying disordered sample was focused at sub-microsecond timescales, without requiring a computer-controlled spatial light modulator or electronic feedback. This was implemented by inserting a pinhole in the mutual focal plane of the two lenses in the degenerate cavity. In this setup, the lasing process found a wavefront that focused the maximum power onto the pinhole in order to minimize loss (FIG. 8c,d). This approach relies on self-organization of the optical field inside the degenerate cavity to create an optimal wavefront that forms a sharp focus from the otherwise randomly scattered light. This wavefront effectively compensates the effect of scattering induced by the random medium. Such wavefront shaping is achieved by all-optical feedback and is therefore orders of magnitude faster than other wavefront-shaping techniques.

Conclusions

Unlike the relatively simple configurations of traditional laser resonators, the configurations and geometries of the unconventional lasers covered in this Technical Review are complex. Despite their differences, one thing these complex lasers have in common is a large number of spatial degrees of freedom, which allows for novel properties and characteristics. By tailoring the spatial structures of lasing modes, their nonlinear interactions within the gain material can be controlled. Consequently, the number of lasing modes and the spatial coherence of emission can be tuned over a wide range. Moreover, the output beams can have arbitrary profile and topology. The different types of complex laser reviewed here each have unique properties and are suitable for various applications with specific requirements, including high-speed speckle-free imaging, spatial coherence gating and focusing through scattering media.

Complex lasers have additional advantages over traditional lasers. Wave-chaotic microcavity lasers and random lasers can suppress spatiotemporal instabilities and chaotic dynamics that are common for high-power lasers[82]. This is because wave interference effects in these lasers disrupt nonlinear processes that form self-organized structures such as filaments, which are inherently unstable, and so the disruption results in stable lasing dynamics. Another example of an advantage is that in multimode fibre lasers, spatiotemporal mode-locking is achieved[83], which paves the way for full control of the spatiotemporal coherence.

The passive schemes for manipulating laser performance using cavity geometry and internal structure could be combined with active control with gain and/or loss[84]. Adaptive shaping of the spatial distribution of the pump intensity enables not only single-mode lasing at any selected wavelength[60,85] but also switching of emission directions[86,87]. A symmetric arrangement of gain and loss in a microcavity (parity–time symmetry) results in stable single-mode operation[88,89]. Optical loss can also induce suppression and revival of lasing in the vicinity of an exceptional point[90,91].

Because complex lasers have numerous degrees of freedom, they may be used for reservoir computing[92]. The self-adaptive nature of a highly multimode laser is exploited for rapid phase retrieval[93]. Imposing constraints in a digital degenerate cavity laser breaks the degeneracy between the transverse modes and forces the system to find a lasing state with minimal loss. In this manner, complex lasers can be mapped to hard computational problems and used as physical simulators[94].

Whereas this Technical Review focuses on the first-order coherence of complex lasers, the second-order or even-higher-order coherence properties are also interesting to explore. In a laser, optical gain saturation suppresses intensity fluctuations of the emission, enhancing the second-order coherence. The nonlinear multimodal interactions can make the higher-order coherence properties of a complex laser very different from those of a conventional laser. Although we have reviewed certain processes and applications of complex laser systems, this Technical Review only hints at the enormous and largely unexplored potential of these systems.

Published online 17 January 2019

1. Chellappan, K. V., Erden, E. & Urey, H. Laser-based displays: a review. *Appl. Opt.* **49**, F79–F98 (2010).
2. Friberg, A. T. & Setala, T. Electromagnetic theory of optical coherence [Invited]. *J. Opt. Soc. Am. A.* **33**, 2431–2442 (2016).
3. Mandel, L. & Wolf, E. *Optical Coherence and Quantum Optics* (Cambridge Univ. Press, 1995).
4. Dainty, J. C. *Laser Speckle and Related Phenomena* Vol. 9 (Springer Science & Business Media, 2013).
5. Goodman, J. W. *Speckle Phenomena in Optics: Theory and Applications* (Roberts and Company Publishers, 2007).
6. Webb, R. H. Confocal optical microscopy. *Rep. Prog. Phys.* **59**, 427–471 (1996).
7. Lowenthal, S. & Joyeux, D. Speckle removal by a slowly moving diffuser associated with a motionless diffuser. *J. Opt. Soc. Am.* **61**, 847 (1971).
8. Redding, B., Allen, G., Dufresne, E. R. & Cao, H. Low-loss high-speed speckle reduction using a colloidal dispersion. *Appl. Opt.* **52**, 1168–1172 (2013).
9. Akram, M. N., Tong, Z. M., Ouyang, G. M., Chen, X. Y. & Kartashov, V. Laser speckle reduction due to spatial and angular diversity introduced by fast scanning micromirror. *Appl. Opt.* **49**, 3297–3304 (2010).
10. Roelandt, S. et al. Human speckle perception threshold for still images from a laser projection system. *Opt. Express* **22**, 23965–23979 (2014).
11. Geri, G. A. & Williams, L. A. Perceptual assessment of laser-speckle contrast. *J. Soc. Inf. Disp.* **20**, 22–27 (2012).
12. Redding, B. et al. Low-spatial-coherence high-radiance broadband fiber source for speckle free imaging. *Opt. Lett.* **40**, 4607–4610 (2015).
13. Arnaud, J. A. Degenerate optical cavities. *Appl. Opt.* **8**, 189–196 (1969).
14. Pole, R. Conjugate-concentric laser resonator. *JOSA* **55**, 254–260 (1965).
15. Nixon, M., Redding, B., Friesem, A. A., Cao, H. & Davidson, N. Efficient method for controlling the spatial coherence of a laser. *Opt. Lett.* **38**, 3858–3861 (2013).
16. Chriki, R. et al. Manipulating the spatial coherence of a laser source. *Opt. Express* **23**, 12989–12997 (2015).
17. Hartmann, S. & Elsäßer, W. A novel semiconductor-based, fully incoherent amplified spontaneous emission light source for ghost imaging. *Sci. Rep.* **7**, 41866 (2017).
18. Stöckmann, H.-J. *Quantum Chaos: An Introduction* (Cambridge Univ. Press, 1999).
19. Cao, H. & Wiersig, J. Dielectric microcavities: model systems for wave chaos and non-Hermitian physics. *Rev. Mod. Phys.* **87**, 61–111 (2015).

20. Bunimovich, L. A. On the ergodic properties of nowhere dispersing billiards. *Commun. Math. Phys.* **65**, 295–312 (1979).
21. Tureci, H. E., Schwefel, H. G. L., Jacquod, P. & Stone, A. D. Modes of wave-chaotic dielectric resonators. *Progress. Opt.* **47**, 75–137 (2005).
22. Redding, B. et al. Low spatial coherence electrically pumped semiconductor laser for speckle-free full-field imaging. *Proc. Natl. Acad. Sci. USA* **112**, 1304–1309 (2015).
23. Heller, E. J. Bound-state eigenfunctions of classically chaotic Hamiltonian systems: scars of periodic orbits. *Phys. Rev. Lett.* **53**, 1515 (1984).
24. Harayama, T. & Shinohara, S. Two-dimensional microcavity lasers. *Laser Photonics Rev.* **5**, 247–271 (2011).
25. Cao, H. Lasing in disordered media. *Prog. Opt.* **45**, 317–370 (2003).
26. Noginov, M. A. & Letokhov, V. S. *Solid-State Random Lasers* (Springer, 2005).
27. Wiersma, D. S. The physics and applications of random lasers. *Nat. Phys.* **4**, 359–367 (2008).
28. Letokhov, V. S. Generation of light by a scattering medium with negative resonance absorption. *Sov. Phys. Jetp* **26**, 835 (1968).
29. Wiersma, D. S. & Lagendijk, A. Light diffusion with gain and random lasers. *Phys. Rev. E* **54**, 4256–4265 (1996).
30. Jiang, X. Y. & Soukoulis, C. M. Time dependent theory for random lasers. *Phys. Rev. Lett.* **85**, 70–73 (2000).
31. Burin, A. L., Ratner, M. A., Cao, H. & Chang, R. P. H. Model for a random laser. *Phys. Rev. Lett.* **87**, 215503 (2001).
32. Vanneste, C. & Sebbah, P. Selective excitation of localized modes in active random media. *Phys. Rev. Lett.* **87**, 183903 (2001).
33. Cao, H. et al. Random laser action in semiconductor powder. *Phys. Rev. Lett.* **82**, 2278–2281 (1999).
34. Cao, H. et al. Ultraviolet lasing in resonators formed by scattering in semiconductor polycrystalline films. *Appl. Phys. Lett.* **73**, 3656–3658 (1998).
35. Lawandy, N. M., Balachandran, R. M., Gomes, A. S. L. & Sauvain, E. Laser action in strongly scattering media. *Nature* **368**, 436–438 (1994).
36. Frolov, S. V., Vardeny, Z. V., Yoshino, K., Zakhidov, A. & Baughman, R. H. Stimulated emission in high-gain organic media. *Phys. Rev. B* **59**, R5284–R5287 (1999).
37. Turitsyn, S. K. et al. Random distributed feedback fibre lasers. *Phys. Rep.* **542**, 133–193 (2014).
38. Siddique, M., Yang, L., Wang, Q. Z. & Alfano, R. R. Mirrorless laser action from optically pumped dye-treated animal-tissues. *Opt. Commun.* **117**, 475–479 (1995).
39. Leong, E. S. P. & Yu, S. F. UV random lasing action in p-SiC(4H)/i-ZnO-SiO_2 nanocomposite/n-ZnO: Al heterojunction diodes. *Adv. Mater.* **18**, 1685 (2006).
40. Hokr, B. H. et al. Bright emission from a random Raman laser. *Nat. Commun.* **5**, 4356 (2014).
41. Liang, H. K. et al. Electrically pumped mid-infrared random lasers. *Adv. Mater.* **25**, 6859–6863 (2013).
42. Schonhuber, S. et al. Random lasers for broadband directional emission. *Optica* **3**, 1035–1038 (2016).
43. Ling, Y. et al. Investigation of random lasers with resonant feedback. *Phys. Rev. A.* **64**, 063808 (2001).
44. Cao, H., Ling, Y., Xu, J. Y. & Burin, A. L. Probing localized states with spectrally resolved speckle techniques. *Phys. Rev. E* **66**, 025601 (2002).
45. El-Dardiry, R. G. S., Mosk, A. P., Muskens, O. L. & Lagendijk, A. Experimental studies on the mode structure of random lasers. *Phys. Rev. A.* **81**, 043830 (2010).
46. Vanneste, C., Sebbah, P. & Cao, H. Lasing with resonant feedback in weakly scattering random systems. *Phys. Rev. Lett.* **98**, 143902 (2007).
47. Gouedard, C., Husson, D., Sauteret, C., Auzel, F. & Migus, A. Generation of spatially incoherent short pulses in laser-pumped neodymium stoichiometric crystals and powders. *J. Opt. Soc. Am. B* **10**, 2358–2363 (1993).
48. Redding, B., Choma, M. A. & Cao, H. Spatial coherence of random laser emission. *Opt. Lett.* **36**, 3404–3406 (2011).
49. Sale, T. E. *Vertical Cavity Surface Emitting Lasers* (Research Studies Press; Wiley, 1995).
50. Huang, K. F., Chen, Y. F., Lai, H. C. & Lan, Y. P. Observation of the wave function of a quantum billiard from the transverse patterns of vertical cavity surface emitting lasers. *Phys. Rev. Lett.* **89**, 224102 (2002).
51. Gensty, T. et al. Wave chaos in real-world vertical-cavity surface-emitting lasers. *Phys. Rev. Lett.* **94**, 233901 (2005).
52. Peeters, M. et al. Spatial decoherence of pulsed broad-area vertical-cavity surface-emitting lasers. *Opt. Express* **13**, 9337–9345 (2005).
53. Mandre, S. K., Elsäßer, W., Fischer, I., Peeters, M. & Verschaffelt, G. Evolution from modal to spatially incoherent emission of a broad-area VCSEL. *Opt. Express* **16**, 4452–4464 (2008).
54. Craggs, G., Verschaffelt, G., Mandre, S. K., Thienpont, H. & Fischer, I. Thermally controlled onset of spatially incoherent emission in a broad-area vertical-cavity surface-emitting laser. *IEEE J. Sel. Top. Quant.* **15**, 555–562 (2009).
55. Riechert, F. et al. Speckle characteristics of a broad-area VCSEL in the incoherent emission regime. *Opt. Commun.* **281**, 4424–4431 (2008).
56. Munro, E. A., Levy, H., Ringuette, D., O'Sullivan, T. D. & Levi, O. Multi-modality optical neural imaging using coherence control of VCSELs. *Opt. Express* **19**, 10747–10761 (2011).
57. Levy, H., Ringuette, D. & Levi, O. Rapid monitoring of cerebral ischemia dynamics using laser-based optical imaging of blood oxygenation and flow. *Biomed. Opt. Express* **3**, 777–791 (2012).
58. Liew, S. F. et al. Intracavity frequency-doubled degenerate laser. *Opt. Lett.* **42**, 411–414 (2017).
59. Bachelard, N., Andreasen, J., Gigan, S. & Sebbah, P. Taming random lasers through active spatial control of the pump. *Phys. Rev. Lett.* **109**, (2012).
60. Liew, S. F., Ge, L., Redding, B., Solomon, G. S. & Cao, H. Pump-controlled modal interactions in microdisk lasers. *Phys. Rev. A.* **91**, 043828 (2015).
61. Cerjan, A. et al. Controlling mode competition by tailoring the spatial pump distribution in a laser: a resonance-based approach. *Opt. Express* **24**, 26006–26015 (2016).
62. Chriki, R. et al. Spatiotemporal supermodes: rapid reduction of spatial coherence in highly multimode lasers. *Phys. Rev. A.* **98**, 023812 (2018).
63. Dhalla, A. H., Migacz, J. V. & Izatt, J. A. Crosstalk rejection in parallel optical coherence tomography using spatially incoherent illumination with partially coherent sources. *Opt. Lett.* **35**, 2305–2307 (2010).
64. Papagiakoumou, E. et al. Functional patterned multiphoton excitation deep inside scattering tissue. *Nat. Photonics* **7**, 274–278 (2013).
65. Redding, B., Choma, M. A. & Cao, H. Speckle-free laser imaging using random laser illumination. *Nat. Photonics* **6**, 355–359 (2012).
66. Hokr, B. H. et al. A narrow-band speckle-free light source via random Raman lasing. *J. Mod. Opt.* **63**, 46–49 (2016).
67. Haeusler, G. in *Encyclopedia of Modern Optics* Vol. 1 (eds Guenther, R. D., Steel, D. G. & Bayvel, L. P.) 114–123 (Elsevier, 2004).
68. Mermillod-Blondin, A., Mentzel, H. & Rosenfeld, A. Time-resolved microscopy with random lasers. *Opt. Lett.* **38**, 4112–4115 (2013).
69. Corle, T. R. & Kino, G. S. *Confocal Scanning Optical Microscopy and Related Imaging Systems* (Acad. Press, 1996).
70. Petran, M., Hadravsky, M., Egger, M. D. & Galambos, R. Tandem-scanning reflected-light microscope. *J. Opt. Soc. Am.* **58**, 661 (1968).
71. Somekh, M. G., See, C. W. & Goh, J. Wide field amplitude and phase confocal microscope with speckle illumination. *Opt. Commun.* **174**, 75–80 (2000).
72. Redding, B., Bromberg, Y., Choma, M. A. & Cao, H. Full-field interferometric confocal microscopy using a VCSEL array. *Opt. Lett.* **39**, 4446–4449 (2014).
73. Liu, C. G., Cao, H. & Choma, M. A. Coherent artifact suppression in line-field reflection confocal microscopy using a low spatial coherence light source. *Opt. Lett.* **41**, 4775–4778 (2016).
74. Sencan, I. et al. Ultrahigh-speed, phase-sensitive full-field interferometric confocal microscopy for quantitative microscale physiology. *Biomed. Opt. Express* **7**, 4674–4684 (2016).
75. Boas, D. A. & Dunn, A. K. Laser speckle contrast imaging in biomedical optics. *J. Biomed. Opt.* **15**, 011109 (2010).
76. Knitter, S. et al. Coherence switching of a degenerate VECSEL for multimodality imaging. *Optica* **3**, 403–406 (2016).
77. Dickey, F. M. & Holswade, S. C. *Laser Beam Shaping: Theory and Techniques* (Marcel Dekker, 2000).
78. Turunen, J., Vasara, A. & Friberg, A. T. Propagation invariance and self-imaging in variable-coherence optics. *J. Opt. Soc. Am. A* **8**, 282–289 (1991).
79. Chriki, R. et al. Rapid and efficient formation of propagation invariant shaped laser beams. *Opt. Express* **26**, 4431–4439 (2018).
80. Chriki, R. et al. Spin-controlled twisted laser beams: intra-cavity multi-tasking geometric phase metasurfaces. *Opt. Express* **26**, 905–916 (2018).
81. Nixon, M. et al. Real-time wavefront shaping through scattering media by all-optical feedback. *Nat. Photonics* **7**, 919–924 (2013).
82. Bittner, S. et al. Suppressing spatiotemporal lasing instabilities with wave-chaotic microcavities. *Science* **361**, 1225 (2018).
83. Wright, L. G., Christodoulides, D. N. & Wise, F. W. Spatiotemporal mode-locking in multimode fiber lasers. *Science* **358**, 94–97 (2017).
84. Andreasen, J. et al. Partially pumped random lasers. *Int. J. Mod. Phys. B* **28**, (2014).
85. Bachelard, N., Gigan, S., Noblin, X. & Sebbah, P. Adaptive pumping for spectral control of random lasers. *Nat. Phys.* **10**, 426–431 (2014).
86. Liew, S. F., Redding, B., Ge, L., Solomon, G. S. & Cao, H. Active control of emission directionality of semiconductor microdisk lasers. *Appl. Phys. Lett.* **104**, (2014).
87. Hisch, T., Liertzer, M., Pogany, D., Mintert, F. & Rotter, S. Pump-controlled directional light emission from random lasers. *Phys. Rev. Lett.* **111**, 023902 (2013).
88. Feng, L., Wong, Z. J., Ma, R. M., Wang, Y. & Zhang, X. Single-mode laser by parity-time symmetry breaking. *Science* **346**, 972–975 (2014).
89. Hodaei, H., Miri, M. A., Heinrich, M., Christodoulides, D. N. & Khajavikhan, M. Parity-time-symmetric microring lasers. *Science* **346**, 975–978 (2014).
90. Liertzer, M. et al. Pump-induced exceptional points in lasers. *Phys. Rev. Lett.* **108**, 173901 (2012).
91. Peng, B. et al. Loss-induced suppression and revival of lasing. *Science* **346**, 328–332 (2014).
92. Brunner, D., Soriano, M. C., Mirasso, C. R. & Fischer, I. Parallel photonic information processing at gigabyte per second data rates using transient states. *Nat. Commun.* **4**, 1364 (2013).
93. Tradonsky, C. et al. Rapid phase retrieval by lasing. Preprint at https://arxiv.org/abs/1805.10967 (2018).
94. McMahon, P. L. et al. A fully programmable 100-spin coherent Ising machine with all-to-all connections. *Science* **354**, 614–617 (2016).
95. Siegman, A. E. *Lasers* (Univ. Sci. Books, 1986).

Acknowledgements

H.C., R.C., A.F. and N.D. acknowledge funding by the United States–Israel Binational Science Foundation (BSF) under grant no. 2015509. R.C., A.F. and N.D. were supported by the Israel Science Foundation (ISF) by grant no. 1881/17. H.C. and S.B. acknowledge support by the US Office of Naval Research (ONR) via grant no. N00014–13–1–0649. H.C. was supported by the US Air Force Office of Scientific Research under grant no. FA9550–16–1–0416.

Author contributions

All authors contributed equally to the preparation of this manuscript.

Competing interests

The authors declare no competing interests.

Publisher's note

Springer Nature remains neutral with regard to jurisdictional claims in published maps and institutional affiliations.